Hybrid Pulsating Heat Pipe for Space Applications with Non-Uniform Heating Patterns: Ground and Microgravity Experiments

D. Mangini[1], M. Mameli[2], D. Fioriti[2], S. Filippeschi[2], L. Araneo[3], M. Marengo[4]

[1]Department of Engineering, University of Bergamo, Dalmine, Italy.
[2]DESTEC, University of Pisa, Pisa, Italy.
[3]Polytechnic of Milan, Milan, Italy.
[4] School of Computing, Engineering and Mathematics, University of Brighton, England.

ABSTRACT

A hybrid Closed Loop Thermosyphon/Pulsating Heat Pipe with an inner diameter bigger than the capillary threshold is tested both on ground and in hyper/microgravity conditions. The device, partially filled up with FC-72, consists of an aluminum tube (inner diameter: 3 mm) bent into a planar serpentine with five curves at the evaporator. A transparent section closes the loop in the condenser zone, allowing fluid flow visualization. Five heaters are mounted alternatively on the branches, just above the turns and controlled independently, in order to investigate the effect of non-uniform heating configurations. On ground, where the device works as a thermosyphon, the non-uniform heating configurations promote the fluid net circulation in a preferential direction, increasing the thermal performance with respect to the homogeneous heating. Parabolic flights point out that during the 20 seconds of microgravity, the sudden absence of the buoyancy force activates an oscillating slug/plug flow regime, typical of the Pulsating Heat Pipes, allowing the device to work also without the assistance of gravity. Furthermore, peculiar heating configurations can shorten the stop-over periods and stabilize the pulsating two-phase flow motion.

Keywords: Thermosyphon; Pulsating Heat Pipe; Microgravity; Non-Uniform Heating.

NOMENCLATURE

BHM: Bottom Heated Mode [-]
Bo : Bond Number [-]
CHF: Critical Heat Flux [W/cm^2]
CPL: Capillary Pumped Loop [-]
d : Diameter [m]
FPGA: Field Programmable Gate Array [-]
FR : Filling Ratio [-]
g : Gravity acceleration [m/s^2]
Ga : Garimella Number [-]
LHP: Loop Heat Pipe [-]
PFC: Parabolic Flight Campaign [-]
PHP: Pulsating Heat Pipe [-]
SPHP: Space Pulsating Heat Pipe [-]
T : Absolute temperature [°C]

THM: Top Heated Mode [-]
TS: Thermosyphon [-]
Q : Heat Power Input [W]
R_{eq} : Equivalent Thermal Resistance [K/W]
Re : Reynolds Number [-]
U : Fluid Velocity [m/s]
We : Weber Number [-]
μ : Dynamic Viscosity [Pas]
ρ : Density [kg/m^3]
σ : Surface Tension [N/m]
$\overline{\Delta T}_{e-c}$: The difference between the evaporator and the condenser average temperatures in the pseudo-steady state conditions [K]

1 INTRODUCTION

In the last decades the miniaturization of electronic circuits, coupled with their ever-increasing performance, results in a dramatic rise in the amount of heat generated per unit volume. In this perspective, the two-phase heat transfer devices achieve more and more importance not only for the high heat flux capability, but also for their compactness, lightweight, high performance and reliability. The Capillary Pumped Loops (CPL) and Loop Heat Pipes (LHP) are already successfully utilized in a variety of space missions for their peculiar advantages [1]. Thanks to a porous capillary inner structure, also known as wick structure, the CPL and LHP are able to transport heat along tortuous and longer paths in a very efficient way, decreasing the temperature gradient between the heated and the cooled zone, too. Nevertheless, the wick structure is not only the most expensive element in the system, but it is also the most difficult one to design and to characterize.

In order to increase the effectiveness to cost ratio, Akachi [2] invented a new kind of passive wickless capillary two-phase loop named Pulsating Heat Pipe (PHP). The PHP consists simply in a capillary tube bent in several U-turns with alternated heated and cooled zones. The device is firstly evacuated and then partially filled-up with the working fluid. The capillary dimension of the tube, making the surface tension forces comparable with respect to the body forces, creates an alternation of liquid slugs and vapor bubbles within the device. The vapor plugs expansion in the heated zone, push the adjacent fluid in the condenser zone, where the condensation of the vapor bubbles permits to release the heat and recall more fluid from the evaporator. These continuous phase change phenomena coupled with the fluid confinement, induce a pulsating and chaotic two-phase flow motion [3, 4] that can be also mantained without any assistance of gravity. This makes the PHP more competitive with respect to the other wickless passive heat transfer devices such as Thermosyphons (TS), since they can be successfully operated both for space applications [5] or, when horizontally oriented, on ground [6]. Nevertheless, being the PHP a relatively young technology, very few studies in microgravity conditions are present in literature. A short review of the main theoretical, numerical and experimental works aiming at understanding the PHP thermal response in microgravity (i.e. by means of Parabolic Flights or Sounding Rockets) provided below.

Delil et al. [7-8] pointed out the theoretical complexity of shifting the design of two-phase devices from normal to microgravity conditions. The first PHP test performed in microgravity conditions was carried out by Kawaji [9] and Gu et al. [10-11]. Two different aluminum prototypes, one straight and one bended, of a flat plate PHP were tested onboard a Falcon 20 aircraft exposing the test rig to ± 0.02g in microgravity and 2.5g in hyper-gravity. Both the prototypes had rectangular cross section channels with

1 mm of hydraulic diameter, charged with R-114. They concluded that under normal and hyper-gravity conditions the Bottom Heated Mode (BHM) leads to smaller temperature difference between the evaporator and the condenser, followed by the middle heating and the Top Heated Mode (THM). In microgravity conditions, the authors stated that all the tested configurations showed better operating and heat transport performance with respect to the normal or hyper-gravity conditions. However, by looking carefully at the results, the increase of performance was evident only for the THM, while the gravity assisted one does not show a sensible temperature reduction during the parabolas.

De Paiva et al. designed and tested a PHP on ground and in a Sounding Rocket Campaign [12,13]. The device, partially filled up with acetone (FR=50%), had 16 turns at the evaporator, while the overall dimensions were 270 x 90 x 250 mm^3. Results showed that their PHP did not reach a steady state condition after the 6 minutes of microgravity, probably due to the large thermal inertia of the cooling system. Anyway, the temperature evolution clearly revealed a self-sustained two-phase flow motion in microgravity. Maeda et al. [14] tested a PHP with check valves to be mounted on a satellite. Even if ground tests showed good results in terms of global heat power input (up to 100 W in horizontal orientation), microgravity tests of such kind of PHP are not yet published in open literature. A transparent Flat Plate PHP allowing a fluid flow visualization of the entire device was tested in microgravity conditions by Ayel et al. [15] onboard the ESA Novespace A300 Zero-G Aircraft. A transparent glass plate was glued on a milled copper block for the flow visualization. The flat plate PHP, with a hydraulic diameter of 2 mm, was charged with water, heated up by means of electrical heaters and cooled using an external liquid circuit. The authors observed that microgravity was generally accompanied by dry-out phenomena at the evaporator section for global heat power inputs higher than 100 W. The sudden decrease of gravity during the parabolic trajectory hindered the return of the refreshed fluid from the top (condenser) to the bottom (evaporator) for the BHM. Nonetheless, both in hyper-gravity and in normal gravity, the gravity field helped the liquid to return to the hot zone rewetting the channel and, thus, recovering the stable operation. Mameli et al. conducted ground and parabolic flight experiments (58^{th} ESA PF campaign) [16], showing that the PHP thermal response due to the occurrence of microgravity conditions in bottom heated mode was very similar to a tilting maneuver from BHM to the horizontal operation on ground. Furthermore, the microgravity tests in horizontal position confirmed a previous numerical analysis [17], suggesting that the PHP performance in zero gravity condition was not different from the horizontal operation on ground in case of planar geometries. Later on, Manzoni et al. [18] proposed an advanced lumped numerical code and the predicted results showed a very good agreement with the experimental thermo-physical behavior during the gravity field transition obtained in [16]. Another test of a PHP in microgravity conditions was performed by Taft et al. [19] by means of Parabolic Flights. An aluminum Flat Plate Pulsating Heat Pipe was tested both on ground and in hyper/microgravity conditions in three different orientations (BHM, Horizontal, THM), different global heat power inputs (450 W, 300 W and 200 W). The device covered a footprint of 25 x 25 cm^2 with 20 U-turns at the condenser zone. Square channels (1.3 x 1.3 mm^2) are milled and the device is partially filled up with acetone. The authors observed that when the device was horizontally placed, the thermal response in microgravity was similar to that one on ground, in line with the results obtained by Mameli et al [17]. Most of the results were reported in terms of the standard equivalent thermal resistance, even if it was not clarified whether 20 seconds of microgravity were sufficient to achieve a steady state regime.

In summary, even if it was demonstrated that PHPs could be a promising solution to dissipate heat also without the assistance of a gravity field, the thermal response in microgravity conditions suggests that the device performance may worsen due to the occurrence of local dry-out conditions at relatively low heating power levels. Therefore, it is mandatory to find a way to avoid dry-out conditions. Assuming

that in microgravity conditions, the critical heat fluxes are lower with respect to the case where gravity assists the flow motion, a straightforward solution could be the increase of the inner diameter (ID). Since the capillary limit is inversely proportional to the gravity field, it is theoretically possible to increase the PHP hydraulic diameter without precluding the formation of a slug/plug flow. The Bond criterion is usually adopted by the PHP community in order to define the confinement diameter (Eq. 1):

$$d_{cr,Bo} = 2\sqrt{\sigma/g(\rho_l - \rho_v)} \quad (1)$$

However, after the start-up, the inertia forces, strictly related to the fluid velocity, play an important role on the fluid confinement and on the flow pattern. For this reason, it is necessary also to take into account the inertial and viscous effects. The dynamic limits based on the Weber number (Eq. 2):

$$d_{We} = 4\sigma/\rho_l U_l^2 \quad (2)$$

and on the Garimella number (Eq.3), as described by Baldassari et al. [20]:

$$d_{cr,Ga} = \sqrt{(160\mu_l/\rho_l U_l)\sqrt{\sigma/g(\rho_l - \rho_v)}} \quad (3)$$

are therefore more suitable to define the limit for space applications, even if further experimental validations are mandatory. In order to provide some order of magnitude, Table 2 shows the confinement diameter both for static and dynamic conditions on ground and in microgravity conditions for FC-72 at 20°C, considering an average fluid velocity of 0.1 m/s, which is a typical order of magnitude of the liquid plugs velocity within a PHP [21].

Even considering the inertial effects, it is therefore possible to test a PHP with an ID slightly higher than the critical one on ground [22,23], opening the frontier to a new family of PHPs that can be named, for sake of simplicity, “Space Pulsating Heat Pipe” (SPHP). Having a larger ID, the main advantage of the SPHP with respect to the conventional PHPs, is the possibility to dissipate higher heat power inputs in microgravity or to run with lower heat fluxes. Such passive thermal device is actually a hybrid system, since it works as a Multi-Evaporator Loop Thermosyphon (MELT) on ground [24] and as a capillary PHP in microgravity conditions. Other successful attempts were also performed by Ayel et al. [25, 26] in hyper/micro gravity conditions by means of parabolic flights. Their Flat Plate Pulsating Heat Pipe was filled up with FC-72, and the hydraulic diameter was 2 mm, which is higher than the capillary static and dynamic thresholds (Table 2). During the PFC, the device was tested in BHM. The authors observed a stratification of the liquid phase both in normal and hyper-gravity conditions, but as soon as microgravity occurred, a slug/plug flow regime was suddenly activated. Furthermore, in weightlessness the authors noticed that the fluid motion was often alternated by some stop-over periods, as also observed by Mangini et al. [23]. In fact, during microgravity, vigorous pulsations were followed by prolonged stop-overs periods. Such stagnant conditions had a negative impact on the heat exchange, and indeed temperatures at the evaporator zone exhibited an increasing trend.

The main outcomes of the works quoted in the above review, are summarized in table 1.

The aim of the present work is to verify whether a particular heating configuration may, on one side, improve its thermal performance on ground and, on the other side, may reduce or even eliminate the stop-over periods in microgravity. For this purpose, a Pulsed Width Modulation (PWM) electronic system is implemented, in order to control independently the five heating elements positioned at the evaporator, so as to vary the heating configuration along the evaporator. The fluid pressure signal

analysis and the flow pattern visualization clearly reveals that an appropriate heating configuration exists for the present test cell.

2 EXPERIMENTAL APPARATUS AND PROCEDURE

The SPHP is made of an aluminum tube (ID/OD 3 mm/5 mm; global axial length: 2550 mm), bent into a planar serpentine with five U-turns at the evaporator zone (all curvature radii are 7.5 mm), as shown in Figure 1a. Two "T" junctions derive two ports at each side: one hosts a pressure transducer (Kulite®, XCQ-093, 1.7 bar abs.), while the second one is devoted to the vacuum and filling procedure. Sixteen "T" type thermocouples (bead diameter of 0.2 mm and an accuracy of ± 0.3 K) are located on the external tube wall: ten in the evaporator zone, six in the condenser zone. The ambient temperature is monitored by means of a thermal resistance (PT 100 Class B sensor RS®). A glass tube (axial length: 50 mm), positioned between the two "T" junctions, allows the fluid flow visualization and closes the loop. A compact camera (Ximea®, MQ013MG-ON objective: Cosmicar/Pentax® C2514-M) is positioned behind the device by means of an aluminum plate, allowing to record the flow evolution inside the glass tube with a resolution of 1280x170 pixel (25 pixel/mm) and a frame rate up to 200 fps. A low vapor pressure epoxy (Varian Torr Seal®) is utilized to seal the "T" junctions as well as the pressure transducer. The condenser section is 165 mm height x 135 width and it is embedded into a heat sink, which is cooled by means of two air fans (Sunon® PMD1208PMB-A), as shown in Figure 1b. Five heating elements (Thermocoax® Single core 1Nc Ac, 0.5 mm O.D., 50 Ω/m, length 720 mm) are wrapped just above the U-turns in the evaporator zone, covering a tube portion of 20 mm each. The position of the heaters is shown in Figure 1c.

The power supply (MW RSP-320) provides an electric power input up to 160 W, corresponding to a wall to fluid radial heat flux up to 17 W/cm^2, with a maximum error of 4.7%. As shown in Figure 2, the power is supplied to the five heaters using a custom electronic interface between the powerlines and the data acquisition/control system (NI-cRIO-9074®). Each heater is managed by an isolated solid-state relay (PVG612A) controlled by the NI 9472 module. The PWM at 10 Hz is used to supply custom power levels to each channel. The actual mean and RMS voltages are measured through a voltage divider in the electronic box and acquired by the NI 9205 module. The camera is triggered at request by control system, and it is synchronized to the pressure measurement through a custom code based on the Field Programmable Gate Array (FPGA) capability embedded in the NI-cRIO-9074®.

Pseudo-steady state[1] conditions can be reached in approximately 3 minutes, due to the low thermal inertia of the heating system and the device. Gravity variations during each parabola are detected by means of a three-axis g-sensor (Dimension Engineering®, DE-ACCM3d). The test cell, consisting of the PHP, the heating and the cooling system, all the sensors, as well as the visualization system, is placed on a beam structure by means of four anti-vibration bushes.

The device is vacuumed by means of an ultra-high vacuum system (Varian® DS42 and TV81-T) down to 0.3 mPa and then it is partially filled up with the working fluid (FC-72) with a volumetric ratio of 0.5 ± 0.03 (corresponding to 8.3 ml) and sealed by means of tin soldering. The fluid itself is previously degassed within a secondary tank, by continuous boiling and vacuuming cycles as described by Henry et al. [27].

A data acquisition system (NI-cRIO-9074®, NI-9264®, NI-9214®, 2xNI-9205®, NI-9217®, NI-9472®) records the output of the thermocouples (at 10 Hz), the pressure transducer (at 200 Hz) and the g-sensor (at 5 Hz). The high-speed camera is connected to an ultra-compact PC (NUC® Board D54250WYB)

[1] Pseudo-steady state conditions are reached when all temperature signals show an average value constant in time.

able to store images up to 200 fps. The video, synchronized with the pressure signal, is recorded for 80 seconds during each parabola and for 30 seconds during the ground tests after reaching steady state conditions. On flight, the movie starts approximately ten seconds before the parabolic maneuver and stops around ten seconds after the second hyper-gravity period.

The bubble velocity is estimated with an open source Particle Image Velocimetry (PIV) software [28] partially modified in order to detect the liquid/vapor interface motion along the transparent section. The sequence of images is saved and cropped on the tube portion of interest. The bubble velocity is furtherly calculated utilizing OpenPIV® software. This software provides an integrated Matlab toolbox for spatial and temporal Particle Image Velocimetry (PIV) data analysis that allows time and spatial analysis, e.g. the velocity profiles of objects in motion. As a convention, the velocity of the bubbles has positive values when the motion is detected from the right to the left of the transparent section; negative in the opposite case. For instance, if the bubble velocity is positive for the majority of the frames recorded, there will be a net circulation in a preferential direction from the right to the left. The time evolution of the menisci velocity reveals how the different heating patterns at the evaporator affect the fluid flow motion both on ground and in microgravity.

The experimental parameters are:
- The total heat input levels, 50 W, 70 W or 90 W which are the sum of all the power levels provided by each of the five heaters;
- The different heating patterns among the five heaters at the evaporator zone;
- The gravity field: normal gravity (1g) during the test on ground and during the straight flight trajectory; hyper-gravity (1.8g) during the ascending and descending maneuvers (duration: 20-25 s each); microgravity during the parabola (duration: 20-21 s).

3 EXPERIMENTAL RESULTS

In this section, results are presented in terms of temperatures and pressure temporal evolutions, while the two-phase flow images recorded both during ground tests and the entire parabola performed are post-processed to find the bubbles velocity during the entire movie. Initially the results obtained on ground, where the device acts as a Multi-Evaporator Loop Thermosyphon, are reported. Then, the more relevant outcomes from the Parabolic Flight Campaign are considered in detail.

3.1 Ground tests

The device has been thermally characterized on ground in BHM with different heating configurations utilizing three different levels of global heat power input: 50 W, 70 W and 90 W. All the heating configurations are kept constant for at least 15 minutes in order to reach pseudo-steady state conditions. The thermal performance of the device is calculated by means of the Equivalent Thermal Resistance defined as follows (Eq. 4):

$$R_{eq} = \frac{\overline{\Delta T}_{e-c}}{\dot{Q}} \quad (4)$$

where $\overline{\Delta T}_{e-c}$ is the difference between the evaporator and the condenser average temperatures in the pseudo-steady state and $\dot{Q}$ is the effective global heat power input provided to the device in the evaporator zone. In the heated branches, here called up-headers, (red arrows in Figure 3), the expansions of vapor bubbles push liquid batches to the condenser. The flow is pumped preferentially by the vapor phase expansion through the straight up-header channels since the U-turns, being a 180° curve that represents fluid-dynamically an important concentrated pressure loss in the system, hinder its pushing in the opposite direction [29]. Then, the refreshed fluid flow can easily return to the evaporator due to gravity by the adjacent branches called down-comers (blue arrows in Figure 3), promoting a two-phase

flow circulation in a preferential direction and refreshing continuously the heated sections, as already demonstrated [24]. Results show that the five independent heaters, supplying different power levels, generate an overall imbalance in the system, which is able to promote a net fluid circulation only for certain heating configurations.

Table 3 shows all the configurations tested on ground providing to the device a global heat power input of 50 W. The Configuration 1, in which all the heating elements dissipate the same heat power input of 10 W, is called "Homogeneous Configuration" and it represents the baseline case useful to compare results with the other "Non-Uniform Configurations" in terms of R_{eq}, temporal evolution of the temperatures and the inner pressure. From the Configuration 2 to the Configuration 5, the power is ever increased from the heater 1 to the heater 5, maintaining however a global heating power of 50 W. These configurations are selected and tested because the fifth heater pumps the fluid for a longer path (i.e. in the horizontal transparent section that closes the loop in the condenser zone) which dissipates a higher heat power. These kind of heating configurations will be named "Increasing" Configurations. Following this line of concept, another configuration (number 6 in Table 3) where the heating power is mostly concentrated only on the fifth heater (26 W that corresponding to the 52% of the global heat power input provided to the device), is called "Local High Value" configuration. Results obtained heating up homogeneously the device points out that the temperature at the lateral branches is lower than the temperature at the central branches, being the transversal thermal conduction lower in this region. Therefore, other two additional configurations (configurations 7 and 8) are tested so as to decrease the heat power provided to the central branches and to increase it at the most lateral ones. These kinds of configuration are named "V-shape" configurations being the heating trend a "V-shape" split between the five heating element, higher at the edges and lower at the center.

Results point out that providing to the device a global heat power input of 50 W, R_{eq} decreases up to 8.7% from the Configuration 2 to the Configuration 5 with respect to the uniform heating configuration (Figure 4a). This is due to a better circulation of the two-phase flow motion in a preferential direction within the device: increasing the heat power input provided to the heater 5, the continue bubble expansions push the liquid batches more vigorously in the horizontal section of the condenser. Nevertheless, by increasing excessively the amount of power provided to the Heater 5 ("Local High Value", Configuration 6) the thermo-fluid behavior gets unstable: the high RMS value (11,8%) in the R_{eq} plot points out continue oscillations of the temperatures both at the evaporator and at the condenser zone, as it is possible to see also from Figure 4b. By increasing the heat power at both of the lateral up-headers ("V-Shape" configurations), the R_{eq} decreases by the 4.1% with respect to the homogeneous heating configuration. Since the most lateral channels are subjected to a lower transversal conduction along the condenser plate with respect to the central channels, the temperature is locally lower at the edges of the condenser when the device is heated up homogeneously. Therefore, heating the most lateral channels with a higher value of power has a beneficial effect on the overall performance of the device, as pointed out by the R_{eq} value obtained with such configuration. Similar results are obtained providing to the device 70 W of global heat power input and testing a specific increasing heating configuration, where the power is continuously increased from the heater 1 to the heater 5. Results highlight that the R_{eq} value in such non-uniform configuration decreases by 0.1 K/W with respect to the homogeneous case, as pointed out by Figure 5 (Homogeneous case) and 6 (Increasing case).

Additionally, a sequence of images (30 seconds at 200 fps) is post-processed to find the liquid/vapor interface velocity between each frame recorded both for the "Increasing" and the homogeneous heating configuration. Results show an improvement of the circulation in a preferential direction from

the right to the left of the transparent section in case of the peculiar non-uniform heating tested. In such configuration, the bubbles move towards the transparent section for the 83% of the time (Figure 6 a and c) in the same direction; while when the device is homogeneously heated up, the circulation is observed for the 63% of the time (Figure 5 a and c). The circulation in a preferential direction has a positive impact on the overall performance, since the heated sections are continuously cooled down by the two-phase flow coming from the condenser, permitting to improve the heat exchange as also already demonstrated by Khandekar et al. [30].

Heating up the serpentine with a global power input of 90 W, the R_{eq} tends to 0.2 K/W for all the configurations. No significant improvement in terms of performance are detectable changing the heating configuration for such global power. As shown in Figure 7, the temperatures both at the evaporator and at the condenser zone are stable for the three heating configurations. This higher global heating power, pushing more vigorously the liquid batches from the evaporator to the condenser, is able to stabilize the thermo-fluid dynamic behavior of the device by means solely of the heating elements non-symmetric position, as already demonstrated by Mameli et al. [24] even for higher global heat power levels. In summary, the peculiar non-uniform heating configuration increases the overall performance especially for the lower global powers tested, as shown in Figure 8.

3.2 Flight tests

Microgravity experiments are carried out onboard the ESA/Novespace Airbus A330, during the 63rd ESA PF campaign. In each flight, a total of 31 parabolic trajectories are performed. Three days of flight are provided in order to carry out experiments. In every day of flight, the first parabola (called parabola zero) is followed by six sequences, each consisting of five consecutive parabolic maneuvers [31]. All sequences are separated by 5 minutes of interval at Earth g-level. Tests are performed by varying the configuration of the heat power input at the evaporator zone. All the configurations tested are pointed out in Figure 9. Being in total 18 different configurations for the 3 days of flight, only the most relevant results obtained in hyper/microgravity conditions are resumed in the experimental result section. The different heat power configurations at the evaporator zone tested are changed during the five minutes' pause at Earth-gravity level between each set of parabola, in order to reach the pseudo-steady state conditions. All the different heat power input configurations are kept constant for the entire set of parabola in order to ensure repeatability. The device is tested in Bottom Heated Mode (BHM).

During the microgravity periods, the sudden absence of the buoyancy forces allows the surface tension force to form menisci, permitting the liquid phase to fill-up completely the tube section and making the device to work as a PHP (Figure 10).

In microgravity, when each of the five heaters dissipates 10 W (Figure 11), the thermo-fluid dynamic of the device shows an "intermittent" behavior: oscillating periods, in which the pressure signal exhibits fluctuations (green sections, Figure 11b) and slug/plug flow motion is observable, are followed by prolonged stop-over periods (red sections in Figure 11b and in Figure 11c). During these stop-over periods, the pressure signal is smooth, while the bubbles in the transparent section stand still in the same position.

Such a stagnant state has a negative impact on the heat exchange, as shown in Figure 11b, where in these moments the temporal evolution of the evaporator temperatures exhibit an increasing trend. When the fluid oscillation recovers, the temperatures tends to stabilize, proving that when the two-phase flow motion is moving in the condenser section, this happens also in the heated zone, dissipating efficiently heat and decreasing the temperatures in the heated sections.

Stop-over periods do not occur providing a "V-Shape" configuration to the device (Figure 12a): the pressure signal fluctuates continuously in microgravity (Figure 12b), while the bubble velocity measurements point out an oscillating flow that never stops (Figure 12c). The constant flow oscillations have a positive effect also for the heat transfer: even if the lateral up-headers dissipates a heating power 40% higher than the uniform case, the maximum temperatures approaches 60°C at the end of the microgravity period. Increasing the heat power inputs at the lateral up-headers, again, since the most lateral channels are subjected to a lower transversal conduction along the condenser plate with respect to the central channels, allows to stabilize the overall thermo-fluid dynamic behavior of the device also in weightlessness.

On ground, the gravity field helps the return of the refreshed two-phase flow from the condenser to the evaporator section through the down-comers, giving a net contribution to the fluid momentum. As a result, the heated sections are continuously refreshed by a two-phase flow with a lower temperature, stabilizing the overall thermo-fluid dynamic behavior of the device. Therefore, even if the up-headers are heated up with non-uniform power levels, the temperatures at the evaporator resides in a narrow range (First hyper-gravity period in Figure 13).

In microgravity, the sudden absence of a gravity field hydro-dynamically "disconnects" the adjacent channels. In fact, the gravity component is one of the more relevant ones in the slug/plug flow momentum equation within PHPs, and it contributes heavily not only in the return of the refreshed fluid from the condenser to the evaporator, but also in the passage of the two-phase flow between adjacent channels, "interconnecting" hydro-dynamically the heated sections [24].

The non-heated branches are not anymore "down-comers" in microgravity, in the sense that in such conditions, the two-phase flow can be pushed between the cooled section and the hot section only by the continue expansions and contractions of the vapor bubbles.

Indeed, after the transition from hyper-gravity to microgravity, the evaporator temperatures tend to spread in a wider range, from 35°C to 70°C, depending on the heating power provided to each element when the device is heated up with an "Increasing" configuration at the evaporator (microgravity period, Figure 13).

As soon as the second hyper-gravity is achieved the two-phase flow is pushed again easily through the down-comers from the condenser to the evaporator, and all the temperatures at the evaporator consequently decrease (second hyper-gravity period, Figure 13).

When the total power level is imposed at 70 W homogeneously distributed, once again, an intermittent working mode is recognizable (Figure 14a): the stop-over periods last up to six consecutive seconds (highlighted with a red rectangle in Figure 14a), and they are followed by sudden pressure peaks. By increasing the power provided to the lateral branches and decreasing it at the center, stop-over periods are another time limited (Figure 14b): the pressure signal oscillates continuously, pointing out a continue flow pulsating slug/plug motion.

Increasing the global heat power input up to 90 W, the homogeneous heating configuration another time alternates stop-overs and intervals in which both the pressure signals and the bubble velocity point out a pulsating motion in microgravity (Figure 15a). Nevertheless, the non-uniform heating configurations tested in microgravity (V-Shape Configuration in Figure 15b and "Increasing" Configuration in Figure 15c) hinder this time the overall thermo-fluid dynamic behavior of the device. During the last seconds of microgravity, the pressure does not oscillate anymore, while the temperatures at the evaporator exhibit an increasing trend, reaching 95 °C at the end of the 20 seconds of microgravity, as if dry out conditions are reached for both the tested non-uniform configurations.

These results seem to be in contradiction with respect to what is pointed out providing to the SPHP

similar non-uniform heating configurations for the 50 W and the 70 W case. However, dry-out conditions are observable only for the channels in which is provided the highest values of heating power. Indeed, a local heating power of 20 W, corresponding to a heat flux of 13 W/cm^2, seems to represent the limit of the SPHP in such conditions for all the configurations, even if further experiments in prolonged weightlessness conditions are necessary to prove the assumption.

Similar results are achieved by providing to the device a global power of 50 W and a "Local High Value" Configuration (Figure 16). In this case, only the TC9, positioned just above the heating element that dissipates locally 26 W, shows an increasing trend during the 20 seconds of microgravity, while all the other channels, heated up with only 6 W, appear stable. The stabilization of the two-phase flow motion occurs especially in the configurations with partial asymmetries, as pointed out in Figure 17, where all the configurations tested in microgravity are divided in three main categories.

Configurations in which alternated stop-over periods and vigorous pulsations are observed, like the homogeneous ones, are colored in orange in Figure 17. Configurations with a dry-out are highlighted in red, while configurations with a flow stabilization are in green. As discussed above, only particular heating configurations are beneficial on the stabilization of the two-phase flow motion in microgravity. The "V-shape" configurations, providing only small asymmetries at the evaporator, are the most effective ones. Either increasing locally the heating power with value higher than 20 W, or varying too much the heating power from the different heaters, causes a local dry-out.

The sudden absence of gravity, hindering the return of the two-phase flow through the down-comers, also establishes dry-out phenomena when just a single branch is heated up with high values of power. Finally, increasing locally the heating power, the subsequent rapid expansion of the vapor bubbles hinders the return of the cooled flow from the condenser, increasing the temperatures and establishing a typical dry-out condition. As a practical conclusion, heating up the channels locally with higher values of heat power at the most lateral branches where the transversal conduction along the condenser plate is lower, in such a way to create a non-symmetric thermal condition at the evaporator, is effective to stabilize the two-phase flow in microgravity. However, increasing excessively the non-symmetric heating configuration, for instance providing the SPHP with the "High Local Value" configuration, the dry-out conditions are more probable than the pumping of the flow into the condenser.

4 CONCLUSIONS

A novel concept of hybrid closed loop Thermosyphon/Pulsating Heat Pipe with an inner diameter higher than the capillary threshold, is tested both on ground and under hyper/microgravity conditions during the 63rd ESA PFC. The thermal device is made by an aluminum tube, bent in order to have five U-turns at the evaporator, partially filled with FC-72. Five heating elements, mounted alternatively just above the U-turns at the evaporator zone, are controlled independently, allowing to test different heating configurations at the evaporator.

- On ground the device works as a two-phase Multi-Evaporator Loop Thermosyphon. Results point out that, heating up the device non-uniformly at the evaporator with peculiar heating configurations, a circulation in a preferential direction is established, with an improvement of the overall thermal performance, especially for the lower heating power tested.
- In microgravity conditions, the sudden absence of the buoyancy force permits to activate a typical PHP oscillating slug/plug flow. The non-heated branches in microgravity are not anymore "down-comers": without gravity, only the continue expansions and contractions of vapor bubbles

move the two-phase flow within the device. It is found that particular non-uniform heating configurations have a beneficial impact also in microgravity.

- The homogeneous heating configuration causes an intermittent working mode when the device is not gravity assisted: stop-over periods are spaced out by vigorous two-phase flow oscillations.
- Increasing the heating power level at the most lateral branches and decreasing it at the center, stop-over periods are limited with respect to the homogeneous heating, establishing a self-sustained pulsating motion during the 20 seconds of microgravity.
- Providing an excessive non-symmetric condition, the branch heated up with the highest power values is affected by dry-out.
- Even if the possibility to stabilize the two-phase flow motion in weightlessness conditions has been proved through certain heating configurations at the evaporator, further experiments in long term microgravity conditions are needed to allow the device to reach steady state conditions.

AKNOWLEDGMENTS

The present work is carried forward in the framework of two projects: the Italian Space Agency (ASI) project ESA_AO-2009 DOLFIN-II and the ESA MAP Project INWIP. We would like to thank Ing. Paolo Battaglia (ASI) for his support, all the great NOVESPACE team in Bordeaux, Dr. Olivier Minster and Dr. Balazs Toth for their interest and support to our PHP activities.

REFERENCES

[1] G. Gilmore, *Spacecraft Thermal Control Handbook*, Fundamental Technologies, The Aerospace Press, El Segundo California (2002).

[2] H. Akachi, Structure of a heat pipe. US Patent 4,921,041, (1990).

[3] Zhang, Y., Faghri, A., Advances and unsolved issues in pulsating heat pipes, *Heat Transfer Engineering*, 29 (2008), 20-31.

[4] Khandekar, S., Groll, M., Charoensawan, P., Terdtoon, P., Pulsating Heat Pipes: Thermo-fluidic Characteristics and Comparative Study with Single Phase Thermosyphon, *Proc. of 12th International Heat Transfer Conference*, Grenoble, France (2004), 459-464.

[5] Gu, J., Kawaji, M., Futamata, R., Effects of gravity on the performance of pulsating heat pipes, *Journal of Thermosphysics and Heat Transfer*, 18 (2004) 370-378.

[6] Charoensawan, P., Terdtoon, P., Thermal performance of horizontal closed-loop oscillating heat pipes, *Applied Thermal Engineering*, 28 (2008), 460-466.

[7] Delil, A. A. M., Microgravity two-phase flow and heat transfer, *Nationaal Lucht- en Ruimtevaartlaboratorium*, 1999.

[8] Delil, A. A. M., Pulsating & oscillating heat transfer devices in acceleration environments from microgravity to supergravity, *Nationaal Lucht- en Ruimtevaartlaboratorium*, 2001.

[9] Kawaji, M. Studies of vibration-induced multi-phase fluid phenomena and pulasating heat pipe performance under microgravity, in *Proc. of the ASME FEDSM'03 - 4th ASME_JSME Joint Fluids Engineering Conference*, Honolulu, Hawaii, USA, 2003.

[10] Gu, J., Kawaji, M., and Futamata, R., Effects of gravity on the performance of Pulsating Heat Pipes, *Journal of Thermophysics and Heat Transfer*, 18 (2004), pp. 370-378.

[11] Gu, J., Kawaji, M., Futamata, R. Microgravity performance of micro pulsating heating pipe, *Microgravity Science and Technology*, 16 (2005), pp. 179-183.

[12] de Paiva, K. V., Mantelli, M. B., H., Slongo, L. K., Burg, S. J., Experimental tests of mini Heat

Pipe, Pulsating Heat Pipe and Heat Spreader under microgravity conditions aboard suborbital rockets, in *Proc. of the 15th International Heat Pipe Conference*, Clemson, South Carolina, USA, 2010.

[13] de Paiva, K., Mantelli, M.B.H., Florez, J.P.M., Nuernberg, G.G.V., Mini Heat Pipe Experiments under Microgravity Conditions. What have we Learned? Proc. of the 17th International Heat Pipe Conference, Kanpur, India, 2013.

[14] Maeda, M., Okamoto, A., Kawasaki, H., Sugita, H., Development of Flat Plate Heat Pipe and the project of on-orbit experiment, in *Proc. of the 41st International Conference on Environmental Systems*, Portland, Oregon, USA, 2011.

[15] Ayel, V., Thevenot, F., Bertin, Y., Romestant, C., Analyse thermo-hydraulique expérimentale d'un caloduc oscillantsous champ de gravité variable, in *Proc. of the Congrès Français de Thermique SFT 2013*, Gerardmer, France, 2013.

[16] Mameli, M., Araneo, L., Filippeschi, S., Marelli, M., Testa, R., Marengo, M., Thermal performance of a closed loop pulsating heat pipe under a variable gravity force, *International Journal of Thermal Science*, 80 (2014), 11-22.

[17] Mameli, M., Marengo M., Zinna, S., Numerical investigation of the effects of orientation and gravity in a Closed Loop Pulsating Heat Pipe. Microgravity Science and Technology, (2012), DOI: 10.1007/s12217-011-9293-2.

[18] Manzoni, M., Mameli, M., De Falco, C., Araneo, L., Filippeschi, S., Marengo, M., Advanced Numerical Method for a Thermally Induced Slug flow: Application to a Capillary Closed Loop Pulsating Heat Pipe, *International Journal of Numerical Methods in Fluids*, in press doi: 10.1002/fld.4222.

[19] Taft, B. S., Laun, F.F., Smith, S., Microgravity Performance of a structurally Embedded Oscillating Heat Pipe, Journal of Thermophysics and Heat Transfer, 29(2) (2015).

[20] Baldassari, C., Marengo, M., Flow boiling in microchannels and minichannels, Progress in Energy and Consumption Science, (2012), 1-36.

[21] Xu, J.L., Li, Y.X., Wong, T.N., High Speed Fow Visualization of a Closed Loop Pulsating Heat Pipe, International Journal of Heat and Mass Transfer, 48 (2005), 3338-3351.

[22] Creatini F., Guidi G.M., Belfi F., Cicero G., Fioriti D., Di Prizio D., Piacquadio S., Becatti G., Orlandini G., Frigerio A., Fontanesi S., Nannipieri P., Rognini M., Morganti N., Filippeschi S., Di Marco P., Fanucci L., Baronti F., Manzoni M., Mameli M., Marengo M., Pulsating Heat Pipe Only for Space: Results of the REXUS 18 Sounding Rocket Campaign XXXIII UIT Congress L'Aquila, Italy, Journal of Physics: Conference Series 655 (2015) 012042 doi:10.1088/1742-6596/655/1/012042.

[23] Mangini, D., Mameli, M., Geourgoulas, A., Araneo, L., Filippeschi, S., Marengo, M., A pulsating heat pipe for space applications: Ground and microgravity experiments, *International Journal of Thermal Sciences*, 95 (2015) 53-63.

[24] Mameli, M., Mangini, D., Vanoli, G. F., Araneo, L., Filippeschi, S., Marengo, M., Advanced Multi-evaporator loop thermosyphon, *Energy*, 112 (2016), 562-573.

[25] Ayel, V., Araneo, L., Scalambra, A., Mameli, M., Romestant, C., Piteau, A., Marengo, M., Filippeschi, S., Bertin, Y., Experimental study of a closed loop flat plate pulsating heat pipe under a varying gravity force, *International Journal of Thermal Sciences*, 96 (2015) , 23-34.

[26] Ayel, V., Araneo, L., Marzorati, P., Romestant, C., Bertin, Y., Marengo, M., Visualizations of the flow patterns in a closed loop flat plate PHP with channel diameter above the critical one and tested under microgravity, *Proc. of 18 International Heat Pipe Conference and 12 International Heat*

Pipe Symposium (2016), South Korea.
[27] Henry, C.D., Kim, J., Chamberlain, B., Heaters size and aspect ratio effects on sub-cooled pool boiling heat transfer in low-g, *Proc. of 3rd International Symposium on Two-Phase Flow Modeling and Experimentation* Pisa, Italy, (2004).
[28] Taylor, Z.J., Gurka, R., Kopp, G.A., Liberzon, M., Long-Duration Time-Resolved PIV to Study Unsteady Aerodynamics, *Instrumentation and Measurement, IEDD Transactions*, 59 (2010) 3262-3269.
[29] Da Silva Lima, R., Thome, J.R., Two-phase flow patterns in U-bends and their contiguous straight tubes for different orientations, tube and bend diameters, *International Journal of Refrigeration*, 35 (2012) 1439-1454.
[30] Kandekhar, S., Dolliger, N., Groll, M., Understanding Operational regimes of closed loop pulsating heat pipes: an experimental study, *Applied Thermal Engineering*, vol. 23, (2002) pp. 707-719.
[31] Novespace A300 Zero-G Rules and Guidelines, Paris, France (2009).

FIGURE CAPTIONS AND TABLES

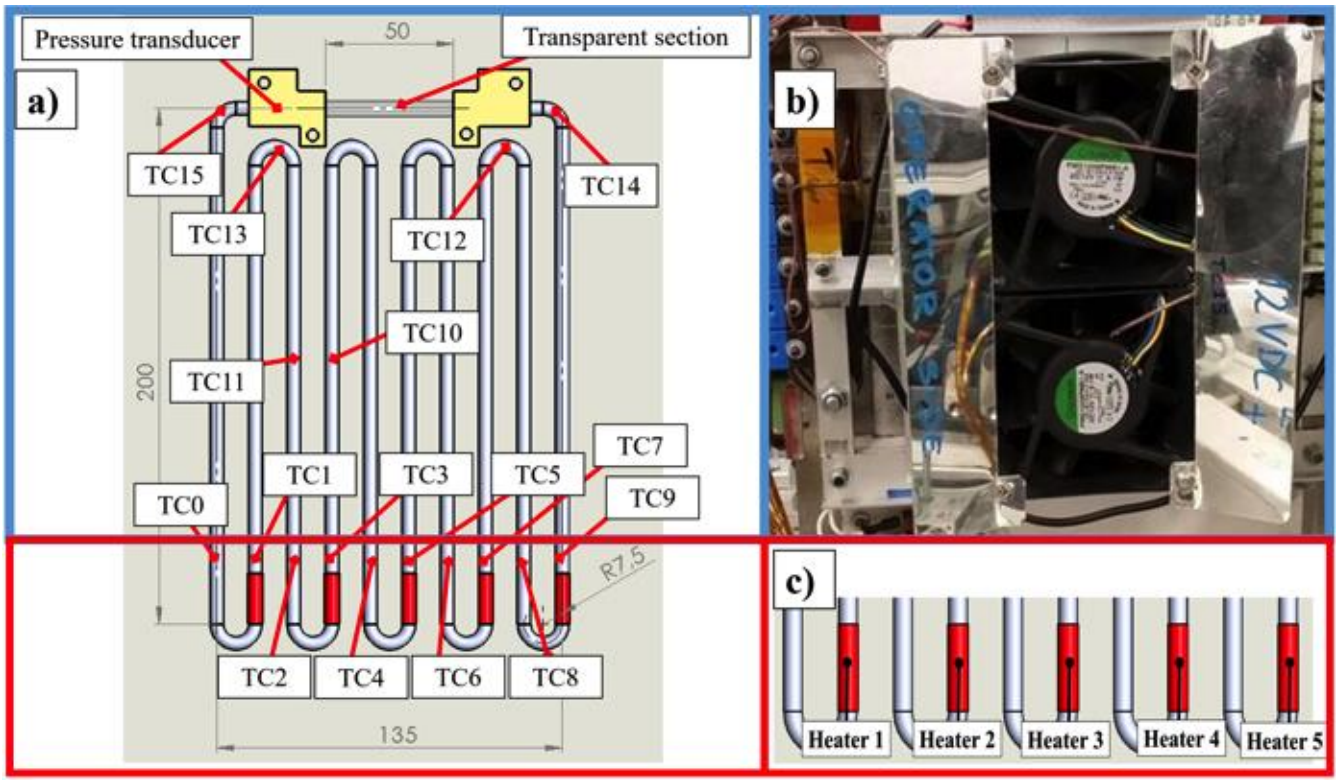

Figure 1. a): thermocouples location along the SPHP tube, b) the condenser zone; c) the 5 heating elements, mounted alternatively just above the U-turns at the evaporator zone.

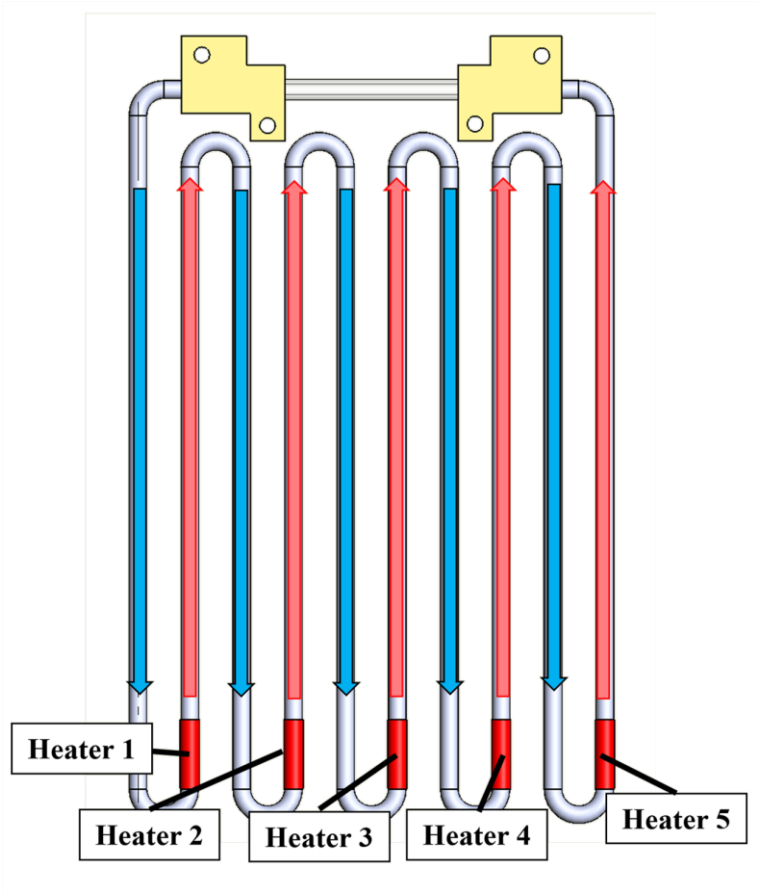

Figure 2. Non-Symmetric heater layout and flow circulation: up-headers highlighted with red arrows; down-comers highlighted with blue arrows.

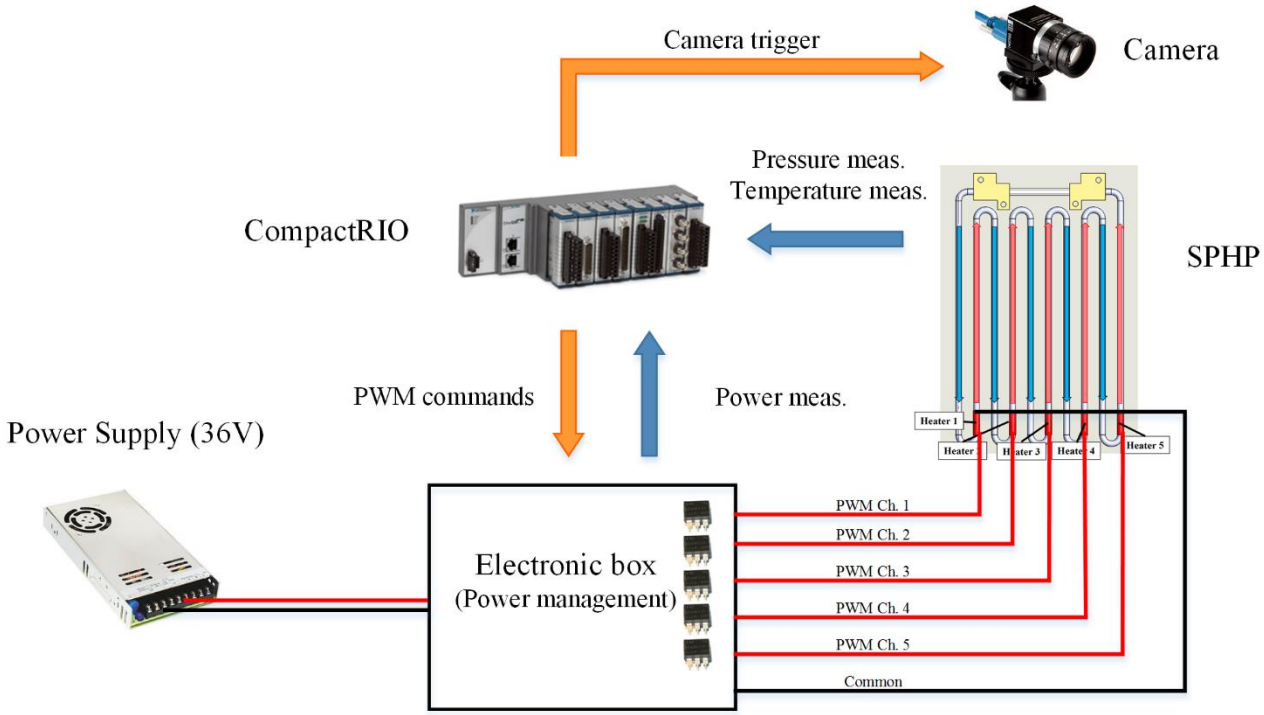

Figure 3 Experimental layout.

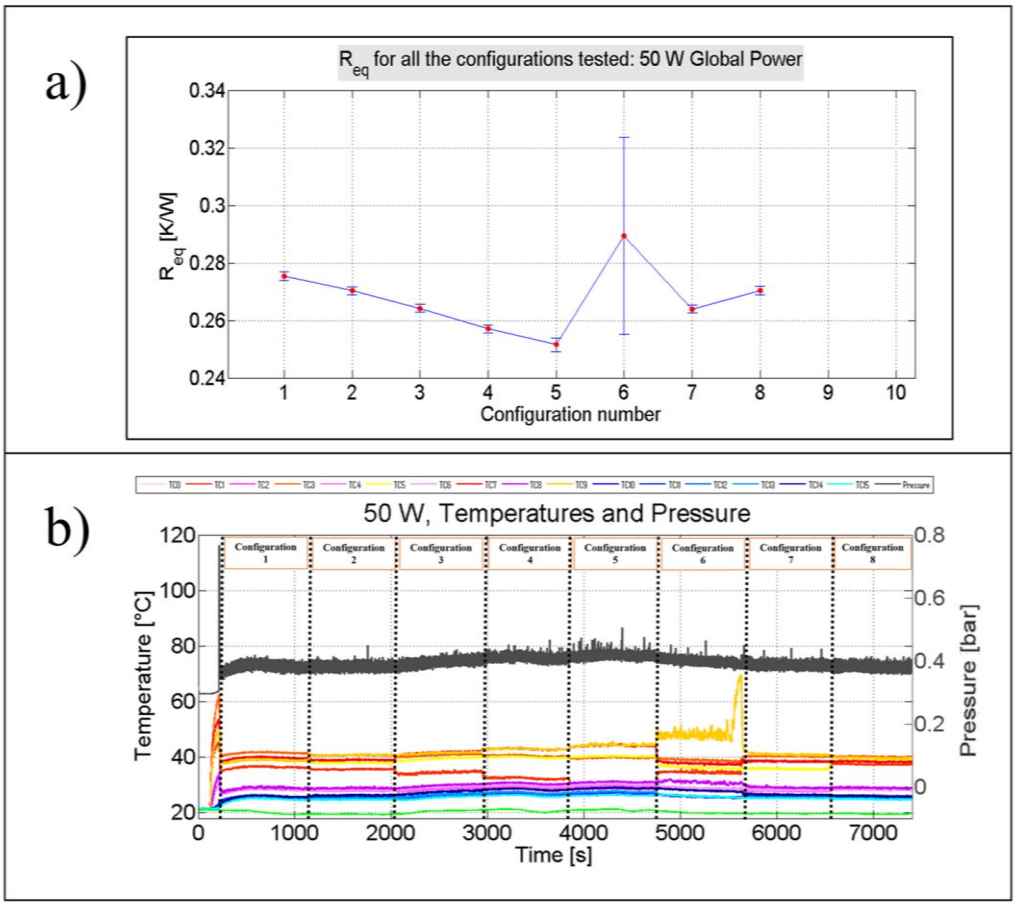

548

549

550 Figure 4. R_{eq} values for the configurations tested on ground providing a global power of 50 W.

551

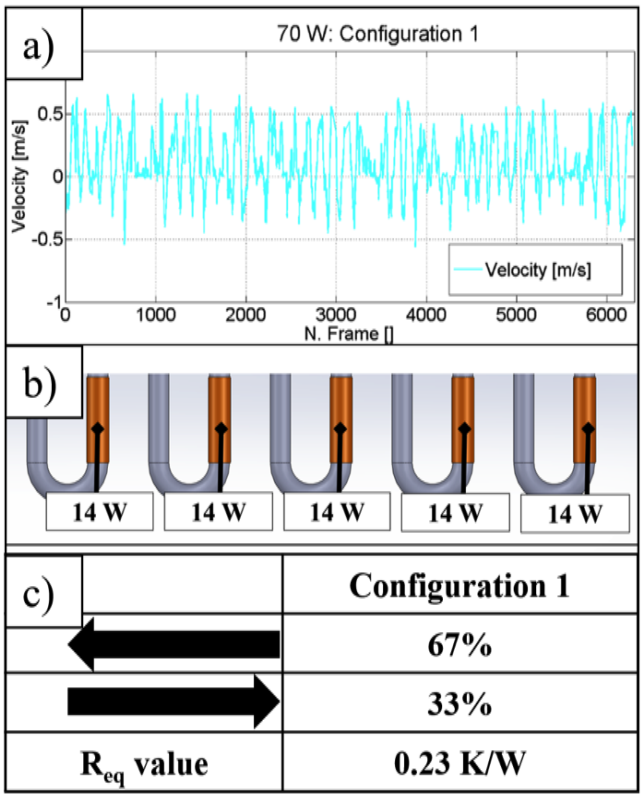

552

553 Figure 5. a) Bubble velocity when the device is heated up uniformly; b) the heating configuration
554 provided; c) Bubble direction and R_{eq} value.

555

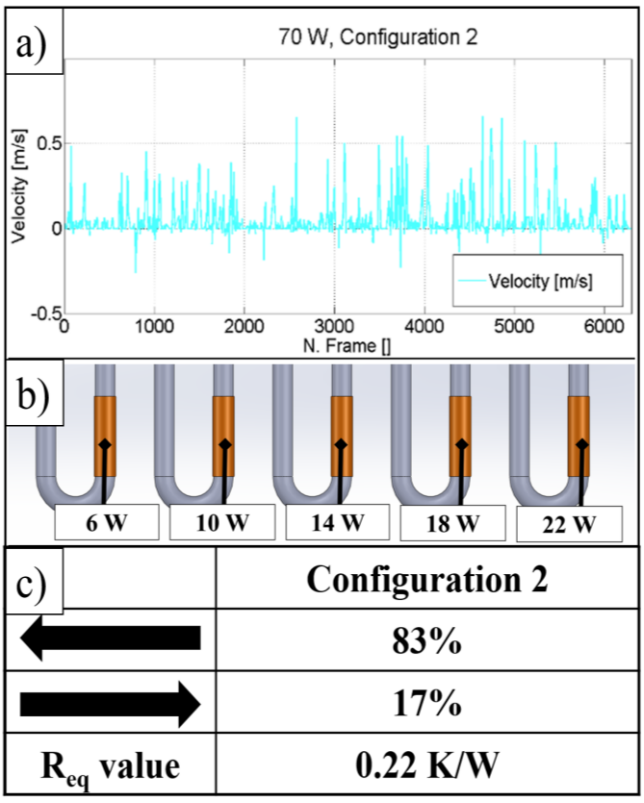

556

557 Figure 6. a) Bubble velocity when the device is heated up non uniform; b) the heating configuration
558 provided; c) Bubble direction and R_{eq} value.

559

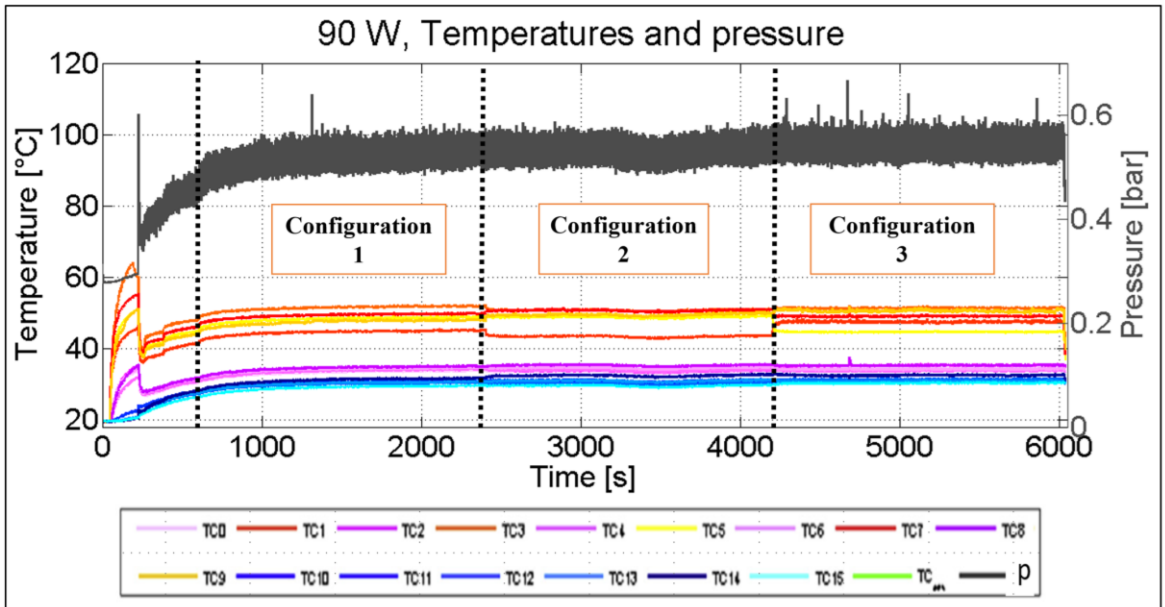

Configuration	Heater 1 [W]	Heater 2 [W]	Heater 3 [W]	Heater 4 [W]	Heater 5 [W]	Req [K/W]
1	18	18	18	18	18	0,21
2	14	16	18	20	22	0,2
3	24	16	10	16	24	0,2

Figure 7. Temperatures and pressure recorded for all the configurations tested on ground utilizing a global power of 90 W.

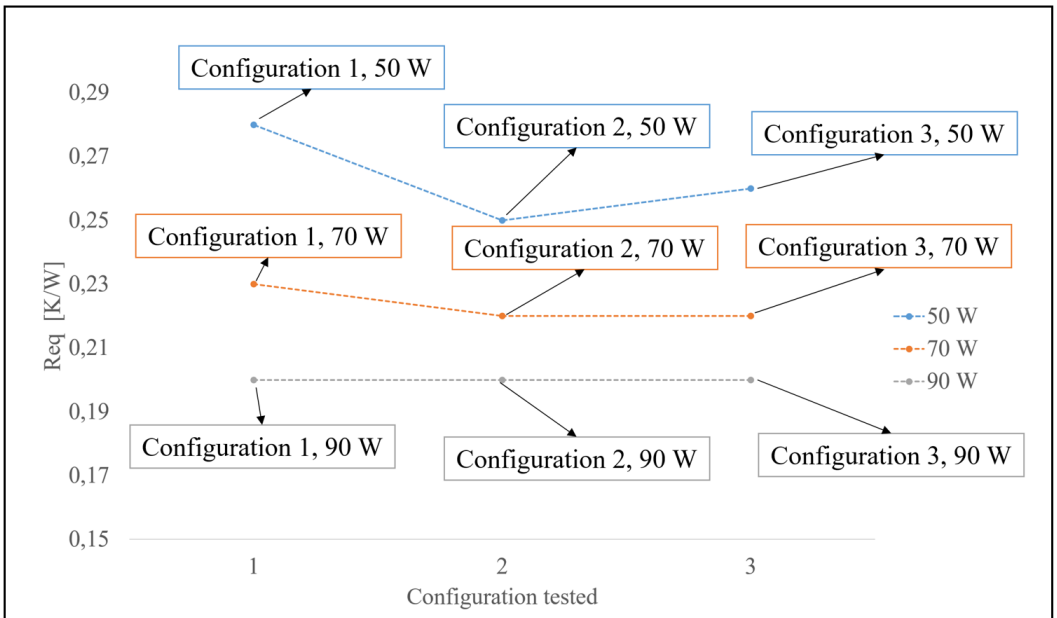

CONFIGURATION	HEATER 1 [W]	HEATER 2 [W]	HEATER 3 [W]	HEATER 4 [W]	HEATER 5 [W]	GLOBAL [W]
1, 50 W	10	10	10	10	10	50
2, 50 W	2	6	10	14	18	50
3, 50 W	14	8	6	8	14	50
1, 70 W	14	14	14	14	14	70
2, 70 W	6	10	14	18	22	70
3, 70 W	18	12	10	12	18	70
1, 90 W	18	18	18	18	18	90
2, 90 W	14	16	18	20	22	90
3, 90 W	24	16	10	16	24	90

Figure 8. R_{eq} values for the main heating configurations tested providing to the device a global heat power input of 50 W, 70 W, 90 W.

	Global Heat power		DAY 1				
			HEATER 1	HEATER 2	HEATER 3	HEATER 4	HEATER 5
			W	W	W	W	W
Heating power configurations	50 W	Homogeneous	10	10	10	10	10
		Local high value 1	9	9	9	9	14
		Increasing 1	6	8	10	12	14
		Increasing 2	4	7	10	14	18
		Increasing 3	2	6	10	14	18
		Local high Value 2	6	6	6	6	25

	Global Heat power		DAY 2				
			HEATER 1	HEATER 2	HEATER 3	HEATER 4	HEATER 5
			W	W	W	W	W
Heating power configurations	50 W	Increasing	2	6	10	14	18
		V-Shape	14	8	6	8	14
		Homogeneous	10	10	10	10	10
	70 W	Homogeneous	14	14	14	14	14
		V-Shape	18	12	10	12	18
		Increasing	6	10	14	18	22

	Global Heat power		DAY 3				
			HEATER 1	HEATER 2	HEATER 3	HEATER 4	HEATER 5
			W	W	W	W	W
Heating power configurations	90 W	Homogeneous	18	18	18	18	18
		V-Shape	22	16	10	16	24
		Increasing	14	16	18	20	22
	50W	W-Shape	12	8	10	8	10
	70 W	V-Shape	18	12	10	12	18
		W-Shape	20	8	14	8	20

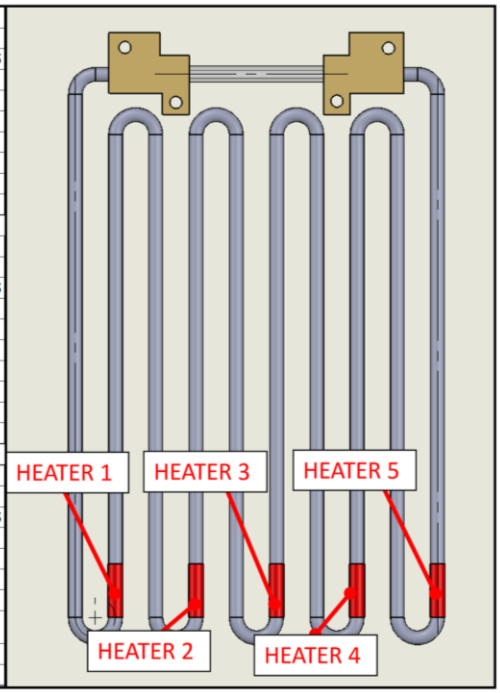

Figure 9. Heating configurations tested during the three days of flight.

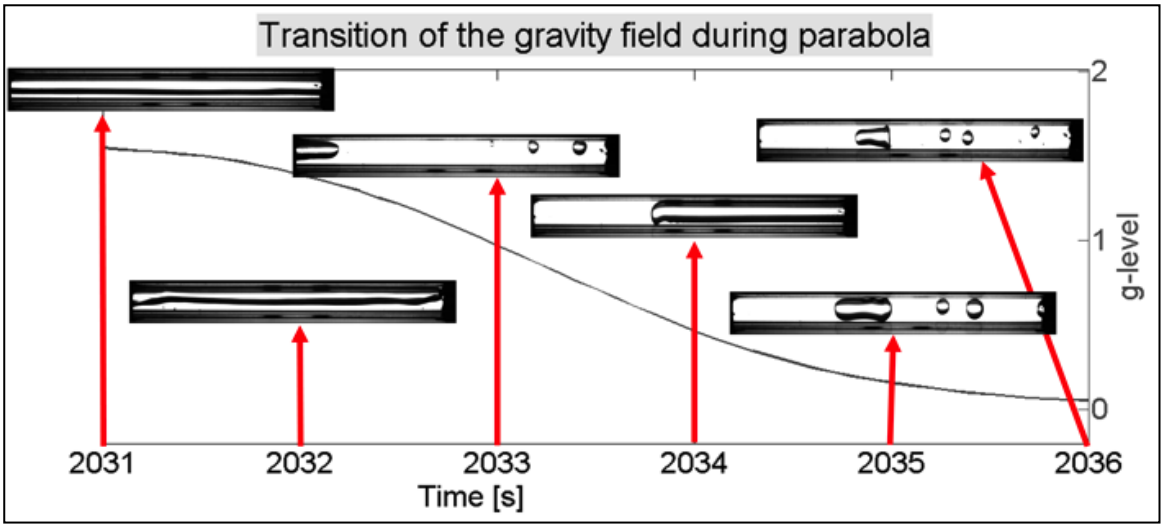

Figure 10. Gravity field transition from hyper to microgravity: activation of a slug/plug flow regime.

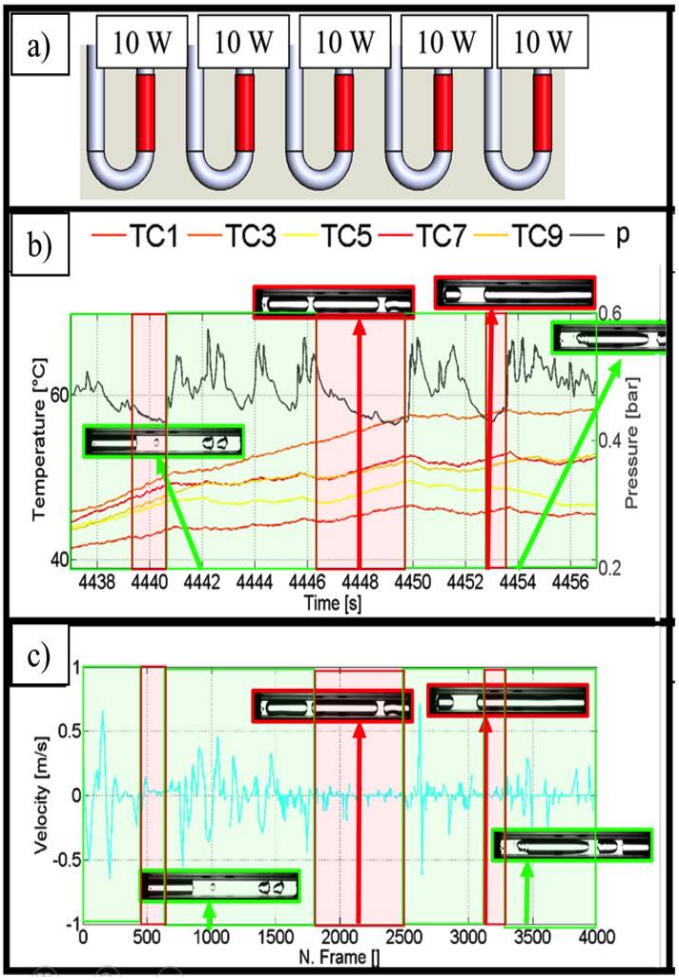

Figure 11. a) Power supplied by the five heating elements: uniform heating pattern; b) Temperatures at the evaporator and pressure during microgravity; c) Bubble velocity measured in microgravity.

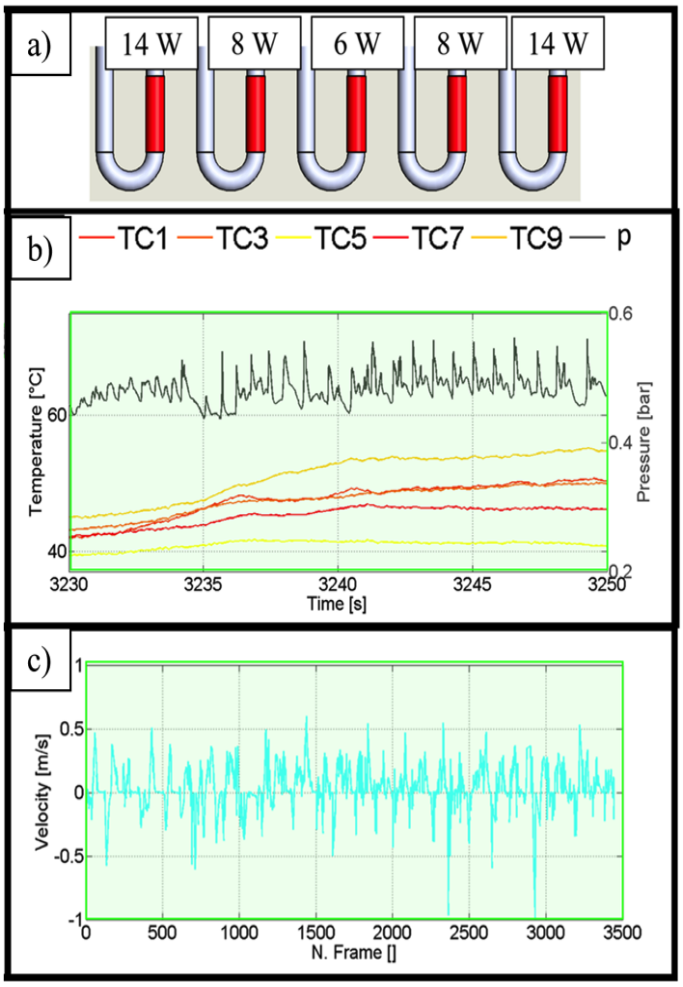

Figure 12. a) Power supplied by the five heating elements: non-uniform heating pattern; b) Temperatures at the evaporator and pressure during microgravity; c) Bubble velocity measured in microgravity.

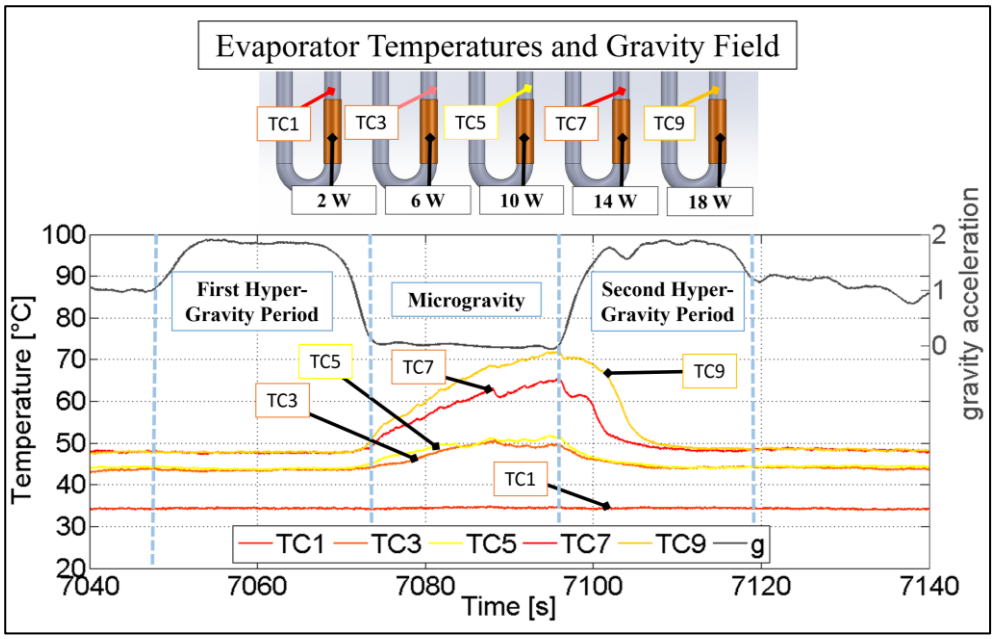

Figure 13. Temperature evolution at the evaporator during parabola.

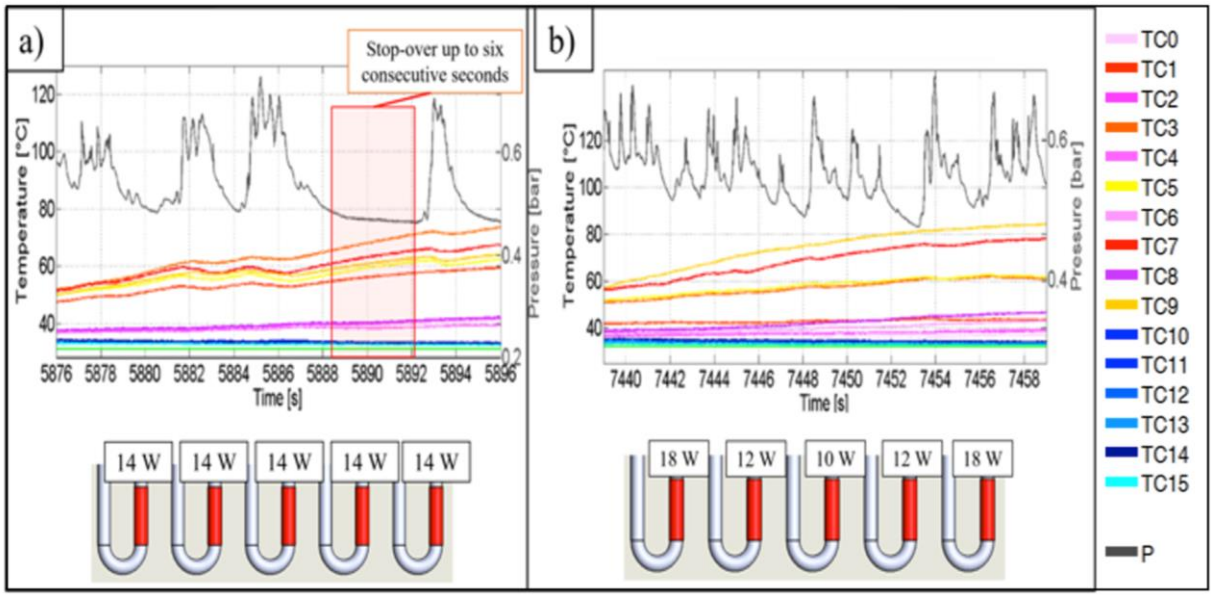

Figure 14. Pressure and temperatures during microgravity providing a global power of 70 W in a) uniform heating and b) non-uniform heating configuration.

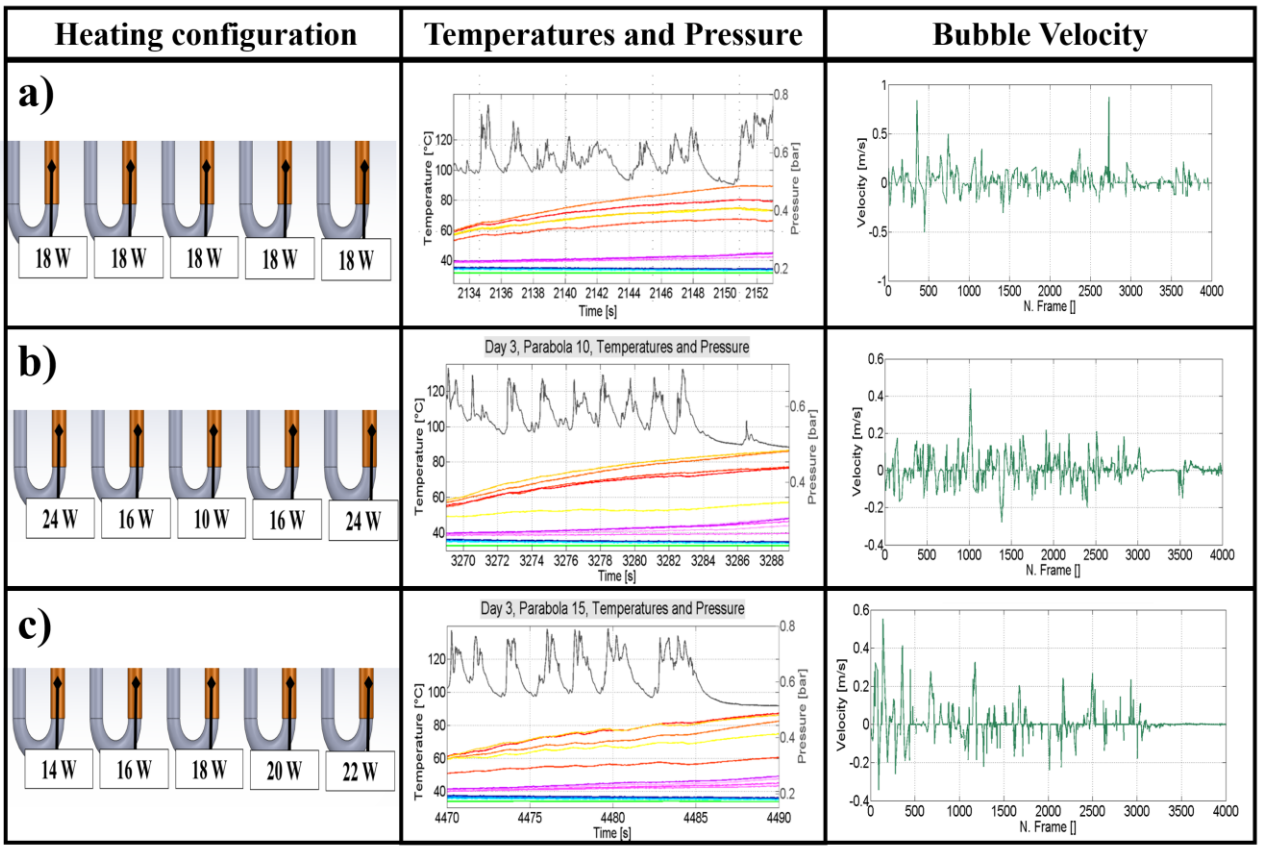

Figure 15. Results in microgravity conditions providing to the device a global heat power input of 90 W for (a) the homogeneous heating configuration; increasing the global heat power input at the most lateral branches (b), continuously increasing the heating power from the heater 1 to the heater 5 (c).

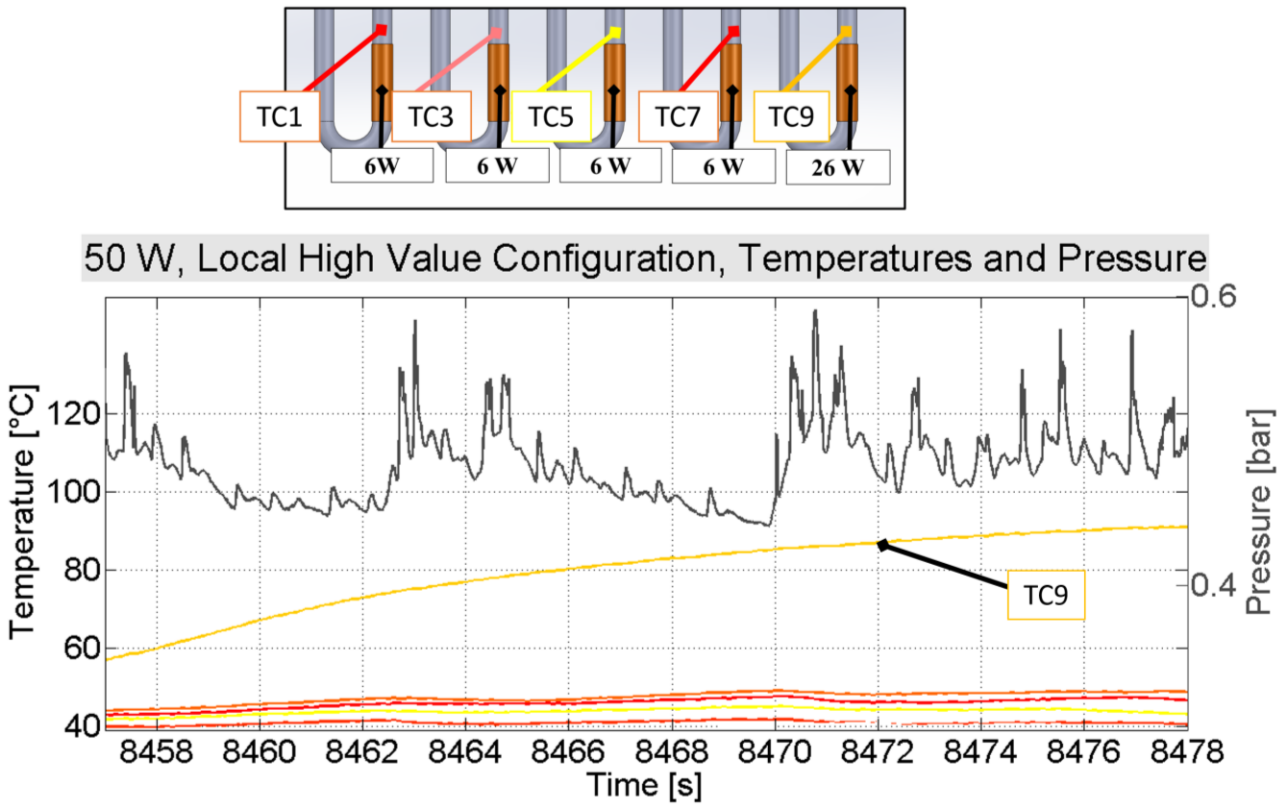

Figure 16. Temporal evolution of the temperatures at the evaporator zone and the inner pressure during the 20 seconds of microgravity providing to the device a Local High Value Configuration (Global heat power input: 50 W).

	Global Heat power		DAY 1				
			HEATER 1	HEATER 2	HEATER 3	HEATER 4	HEATER 5
			W	W	W	W	W
Heating power configurations	50 W	Homogeneous	10	10	10	10	10
		Local high value 1	9	9	9	9	14
		Increasing 1	6	8	10	12	14
		Increasing 2	4	7	10	14	18
		Increasing 3	2	6	10	14	18
		Local high Value 2	6	6	6	6	25

	Global Heat power		DAY 2				
			HEATER 1	HEATER 2	HEATER 3	HEATER 4	HEATER 5
			W	W	W	W	W
Heating power configurations	50 W	Increasing	2	6	10	14	18
		V-Shape	14	8	6	8	14
		Homogeneous	10	10	10	10	10
	70 W	Homogeneous	14	14	14	14	14
		V-Shape	18	12	10	12	18
		Increasing	6	10	14	18	22

	Global Heat power		DAY 3				
			HEATER 1	HEATER 2	HEATER 3	HEATER 4	HEATER 5
			W	W	W	W	W
Heating power configurations	90 W	Homogeneous	18	18	18	18	18
		V-Shape	22	16	10	16	24
		Increasing	14	16	18	20	22
	50W	W-Shape	12	8	10	8	10
	70 W	V-Shape	18	12	10	12	18
		W-Shape	20	8	14	8	20

Figure 17. Thermo-fluid dynamic response of the device in microgravity.

Table 1. Main numerical, theoretical and experimental works of PHPs in microgravity.

Principal Investigator (year)	Exp./Num. /Theor.	Adopted Facility	PHP Layout	Internal diameter/ Fluid	Conclusions
Delil [7] (1999)	Theor.	-	-	[-]	Scaling of two-phase devices from normal to microgravity is complicated. Only distorted scaling offers some possibilities, when not the entire loop but only sections are involved.
Delil [8] (2001)	Theor.	-	-	[-]	The author proposed (but did not furtherly build) a test rig for modified gravity experiments.
Kawaji [9] (2003)	Exp.	Parabolic Flight	One straight and one bended PHP		All the configurations tested, especially the top heating mode PHPs, show better operating characteristics and improved heat transfer under

					reduced gravity. Nevertheless, deeply looking to the results, this is evident only when the PHP is tested in anti-gravity mode.
Gu et al. [10] (2004)	Exp.	Parabolic Flight	One straight and one bended PHP	Square 1 x 1 mm / R114	All the configurations tested for both the heat pipes show better operating characteristics and improved heat transfer under reduced gravity than under normal or hyper-gravity. However, deeply looking to the results, this is evident only when the PHP is tested in anti-gravity mode.
Gu et al. [11] (2005)	Exp.	Parabolic Flight	Transparent Bottom Heated Mode PHP + One straight and one bended PHP	1.6 mm /R114 1 x 1 mm/ R134a	Steady pulsating flows could be achieved under reduced gravity, while hyper-gravity weakens the pulsating motion. Best performance of the tested devices under microgravity. However, deeply looking to the results, this is evident only when the PHP is tested in anti-gravity mode.
de Paiva et al. [12] (2010)	Exp.	Sounding rocket	PHP	1.27 mm/ acetone	The test rig has been built and tested in normal gravity. Sounding rocket has been postponed.
De Paiva et al. [13] (2013)	Exp.	Sounding rocket	PHP	1.27 mm/ acetone	A PHP was tested aboard of a sounding rocket. Even if this work represents the first successful attempt to test a PHP in prolonged microgravity conditions, pseudo-steady state conditions are not reached during the 6 minutes of microgravity.
Maeda et al. [14] (2011)	Exp.	Satellite	3D PHP with check valves	0.8 mm/ R-134a	The prototype has been build and tested in normal gravity. Experiments on satellite are scheduled.
Ayel et al. [15] (2013)	Exp.	Parabolic Flight	Transparent Flat Plate PHP	2 x 2 mm/ water	Dry out occurs during microgravity; an improvement of the thermal performance during hyper-gravity is assisted. Results suffered from leakage between parallel channels.
Mameli et al. [16] (2012)	Num.	-	PHP	2 mm / ethanol	Reduced gravity worsens the performance of the device in BHM. A horizontal PHP behaves as a PHP at 0g.
Mameli et al. [17] (2014)	Exp.	Parabolic Flight	PHP	1,1 mm /FC-72	Horizontal PHP performance is not affected by the gravity field variation occurring during the parabolic trajectories. In the bottom heated mode, the PHP never showed a better heat transfer under reduced gravity. Further ground tests point out analogies between the PHP behavior obtained on ground testing it horizontally and in microgravity conditions.
Manzoni et al. [18] (2016)	Exp./Num.	Parabolic flights	PHP	1,1 mm / FC-72	An advanced hybrid lumped parameter code for the PHP simulation is developed able to simulate transient gravity field variation. Numerical results are

					compared with the PHP thermal behaviour during the variation of the gravity field obtained for a similar device in a previous parabolic flight campaign, showing good agreement.
Taft et al. [19] (2015)	Exp.	Parabolic Flight	FPHP	1.3 x 1.3 mm/ acetone	For conditions in which the proposed FPHP is terrestrially orientation-independent, it is also likely to be gravity-independent, and for conditions in which the device is not terrestrially orientation-independent, it is likely to perform better in microgravity than in a terrestrial environment.
Creatini et al. [22] (2016)	Exp.	Sounding Rocket	Hybrid Closed Loop Thermosyphon/ PHP (SPHP concept)	1,7 mm and 3,0 mm / FC-72	A similar SPHP with respect to that one proposed by Mangini et al. was tested onboard the ESA REXUS Sounding Rocket. Unfortunately the de-spin system of the rocket malfunctioned and the consequent centrifugal acceleration did not allow to reach the capillary regime.
Mangini et al. [23] (2015)	Exp.	Parabolic Flight	Hybrid Closed Loop Thermosypho/P HP (SPHP concept)	3,0 mm / FC-72	In bottom heated mode, the device works as thermosyphon in normal and hyper-gravity conditions, as PHP in reduced gravity. Even if the ID is higher the capillary one on ground, the sudden absence of buoyancy forces in microgravity activated a slug plug flow motion.
Ayel et al. [25] (2015)	Exp.	Parabolic Flight	Flat Plate PHP	1.6 x 1.7/ FC-72	The device in vertical position is influenced by variations in the applied gravity field. Microgravity increases the temperature at the evaporator, worsening the two-phase flow motion, even if the PHP continues working. No important effects are detected in horizontal position.
Ayel et al. [26] (2016)	Exp.	Parabolic Flight	Flat Plate Hybrid Closed Loop Thermosyphon/ PHP	2.5 x 2.5/ FC-72	A transparent flat plate PHP with ID higher than the capillary limit is tested in hyper/micro gravity conditions by means of Parabolic flights in vertical orientation. During normal and hyper-gravity phase the flow appears stratified; in microgravity the fluid distributed naturally in a slug/plug flow pattern. Dry out periods are recognizable in microgravity.

606 Table 2. Confinement diameters for FC-72 at 20 °C both in static and dynamic conditions, on ground
607 and microgravity conditions.

FC-72 (properties at 20°C)	$D_{cr,Bo}$ [mm] (static)	D_{Ga} [mm] with U_l=0.1 m/s
Earth gravity: g=9.81 m/s^2	1.68 mm	0.75 mm

Microgravity: g=0.01 m/s^2	52.88 mm	4.23 mm

608

609 Table 3. Heating configurations tested on ground providing to the device a global heat power input of 50
610 W.

CONFIGURATION	HEATER 1 [W]	HEATER 2 [W]	HEATER 3 [W]	HEATER 4 [W]	HEATER 5 [W]	GLOBAL [W]
1	10	10	10	10	10	50
2	9	9	9	9	14	50
3	6	8	10	12	14	50
4	4	7	10	13	16	50
5	2	6	10	14	18	50
6	6	6	6	6	26	50
7	14	8	6	8	14	50
8	12	8	10	8	12	50

611